Impurity-induced magnetization in a three-dimensional antiferromagnet at the quantum critical point

Y. A. Kharkov,[1,*] I. S. Terekhov,[1,2,3] and O. P. Sushkov[1]
[1]*School of Physics, University of New South Wales, Sydney 2052, Australia*
[2]*Novosibirsk State University, Novosibirsk 630090, Russia*
[3]*Budker Institute of Nuclear Physics, Novosibirsk 630090, Russia*
(Received 31 July 2015; revised manuscript received 11 September 2015; published 13 October 2015)

We consider a single impurity with spin S embedded in a three-dimensional antiferromagnetic system which is close to the quantum critical point (QCP) separating magnetically ordered and disordered phases. Approaching the QCP from the disordered phase, we study the spatial distribution of the spin density and staggered magnetization induced by the impurity. Using two methods (self-consistent Born approximation and renormalization group), we found a power-law decay of the spin density $\propto 1/r^3$, and of the staggered magnetization $\propto 1/r$ with relevant logarithmic corrections. We demonstrate that the local spin at the impurity's site, $r = 0$, approaches to zero at the QCP. We show that in the semiclassical limit of large S the problem is equivalent to the exactly solvable independent boson model. Our results demonstrate existence of spin-charge separation in three-dimensional systems at the QCP.

DOI: 10.1103/PhysRevB.92.155122 PACS number(s): 05.30.Rt, 75.50.Ee, 75.40.Gb

I. INTRODUCTION

Quantum critical phenomena is extensively developing subject in modern condensed matter physics, in both theoretical and experimental frontiers [1]. The most vivid manifestations of quantum phase transitions (QPT) arise in low-dimensional systems such as cuprates and iron pnictides. However, quantum critical behavior is also found in three-dimensional (3D+time) systems. A well-known example of a 3D compound with a magnetic quantum critical point (QCP) is $TlCuCl_3$ [2]. Under normal conditions, the material is in the magnetically disordered phase, while pressure drives QPT to the antiferromagnetically ordered Neel phase.

The quantum critical properties of a system can be significantly influenced by the presence of impurities. For instance, substitution of Cu atoms in the parent compound $TlCuCl_3$ with low concentration of nonmagnetic Mg impurities creates an uncompensated spin $1/2$ at the sites of the impurities, which induces magnetization around the impurities and even leads to the formation of a long-range magnetic order in the macroscopic volume of the crystal [3]. In the magnetically disordered phase, the magnetization cloud around each impurity exponentially decays over a few lattice spacings from the impurity. However, in the vicinity of the QCP, the effect of impurity-induced magnetization can be notably enhanced. Experimental observations reveal an interplay between the impurity-induced staggered magnetization and a quantum criticality near the QCP [4–6].

Despite of the vast amount of theoretical work on the impurity-induced magnetization in quasi-1D and 2D systems (see Refs. [7–12] and references therein), we are not aware of similar studies in the relation to 3D materials. In the present paper, we consider a single impurity with spin S embedded in a 3D antiferromagnet (AF), which is close to the QCP, separating magnetically disordered and magnetically ordered phases. Conceptually, the problem is similar to the Kondo effect (see, e.g., Refs. [13–15]), since, as we show below, the spin cloud screens the impurity's spin at the QCP. While sometimes this phenomenon is called Bose-Kondo effect [16], of course, it is significantly different from the usual Kondo problem, for instance, there are no mobile fermions in our case. In the present work, we study the spatial distribution of the nonlocal spin density and the staggered magnetization induced by the impurity using effective field theory formalism. We show that when approaching the QCP from the disordered phase, the spin density around the impurity decays as $\propto 1/r^3$ with logarithmic corrections and the total spin accumulated in the delocalized cloud is equal to S. We also demonstrate that the induced staggered magnetization decays as $\propto 1/r$.

Closely related to the problem of impurity-induced spin density and impurity-induced Neel order is the phenomenon of spin-charge separation (SCS). The conventional definition of SCS relies on the existence of two quasiparticles carrying spin and charge ("spinon" and "holon"), which is the case in 1D Tomonaga-Luttinger liquid of strongly interacting electrons [17,18]. By contrast, in higher spatial dimensions, there are no known systems with SCS in the conventional definition. However, SCS exists in 2D models, such as hole-doped AF [19–22]. Furthermore, recent research [23] reports pronounced SCS in the vicinity of the magnetic QCP. In the latter case, the precise meaning of SCS is different from SCS in a Tomonaga-Luttinger liquid. A hole creates a spin cloud around the charge with a radius which diverges at the QCP. As a result, the hole's spin becomes delocalized and spatially separated from the impurity's charge pinned to the impurity's site, which basically means SCS. In the present article we show that such SCS also occurs in 3D systems near the QCP.

The paper is organized in the following way. In Sec. II, we introduce an effective field theory describing a 3D AF doped with a single impurity in the vicinity of the QCP. Considering the interaction of the doped AF with a probe magnetic field, we introduce an operator of the spin density and explain how we calculate the induced spin density. Here, we also provide a method of calculation of the staggered magnetization

*y.kharkov@gmail.com

around the impurity. The rest of the paper is divided into two parts, which corresponds to the two techniques of the calculations: self-consistent Born approximation (SCBA) and renormalization group (RG) approach in $3+1$ dimensions. Section III refers to the calculation of the spin density in SCBA for the most physically interesting case of the impurity with spin $S = 1/2$. In Sec. IV, we again calculate the impurity-induced nonlocal spin density, the local spin of the impurity and the staggered magnetization using the RG technique. We also consider the semiclassical limit of an impurity with a large spin. We draw our conclusions in Sec. V.

II. EFFECTIVE THEORY

An example of a 3D lattice model, which incorporates the main features of magnetic quantum criticality, is presented in Fig. 1. The model corresponds to a cubic lattice AF consisting of spins $S = 1/2$ at each site with weak J bonds and strong J' bonds. The system has a QCP driven by parameter $g = J'/J$ and located at $g_c = 4.013$, which separates the disordered magnetic phase of spin dimers at $g > g_c$ from the Neel phase at $g < g_c$ [24,25]. This lattice model describes various properties of $TlCuCl_3$ near the pressure-driven QCP in zero and nonzero magnetic field [24].

Substitution of a $S = 1/2$ Cu^{2+} ion with a spinless Mg^{2+} creates a vacancy (hole). This is shown in Fig. 1. The vacancy acts as an effective impurity with spin $S = 1/2$. The vacancy in the lattice induces a nonlocal magnetization cloud around the impurity site. In the present paper, we will calculate the spatial distribution of the spin density and the staggered magnetization in the spin cloud around the impurity.

The magnetic properties of the critical system are determined by low-energy magnetic excitations. The magnetic excitations are magnons in the Neel phase and triplons in the paramagnetic phase. Hereafter, we use the term magnons for both types of quasiparticles. The effective theory that describes magnons in the vicinity of the QCP is based on the following

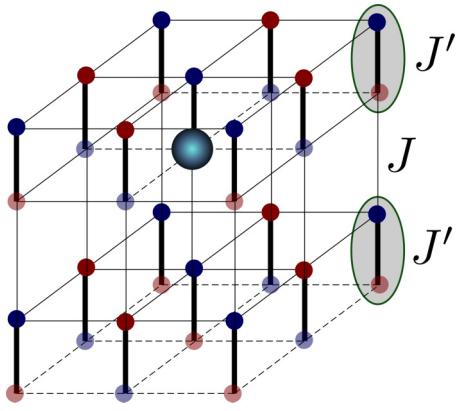

FIG. 1. (Color online) An example of a lattice model for 3D AF with O(3) QCP. Spins $S = 1/2$ located at each site. Thin lines denote weak J bonds and thick lines denote strong J' bonds. A quantum phase transition between the Neel and the dimerized paramagnetic phases occurs at $(J'/J)_c = 4.013$ [24,25]. The big blue sphere represents an impurity (hole) introduced into the lattice.

Lagrangian, see, e.g., Ref. [26]:

$$\mathcal{L}_M = \frac{(\partial_t \boldsymbol{\phi})^2}{2} - \frac{(\nabla_i \phi_\mu)^2}{2} - \frac{\Delta_0^2 \boldsymbol{\phi}^2}{2} - \frac{\alpha_0 (\boldsymbol{\phi}^2)^2}{4!}, \quad (1)$$

where $\phi_\mu = (\phi_x, \phi_y, \phi_z)$ is the magnon field, $\Delta_0^2 \propto g - g_c$ is the magnon gap (squared), α_0 is a four-magnon coupling constant, ∂_t is the time derivative, $\nabla_i = \partial/\partial r_i$ is the three-dimensional gradient. Hereafter, we set the Plank constant and magnon speed equal to unity $\hbar = c = 1$. In the disordered magnetic phase, $\Delta_0^2 > 0$. Near the QCP, the magnon gap $\Delta_0 \to 0$.

The Lagrangian (1) contains quadratic terms as well as quartic term $\propto \phi^4$, describing the magnon self-action. The magnon self-action results in the renormalization of the magnon gap Δ_0 in the Lagrangian (1). From one-loop RG calculations [26] it follows that in the disordered phase, the evolution of the renormalized gap is given by

$$\Delta^2 \propto \Delta_0^2 \left[\ln \frac{C(\Lambda)}{g - g_c} \right]^{-\frac{N+2}{N+8}}, \quad (2)$$

where $N = 3$ in the present case of the O(3) universality class system, and $C(\Lambda)$ is a positive constant, determined by an ultraviolet scale Λ. Besides that, the ϕ^4 term leads to a renormalization of the magnon quasiparticle residue [26]. However, the change of the residue appears only in the two-loop renormalization group, and therefore is small. Hence, for our purposes, we drop out the self-action term from the Lagrangian (1) and substitute the bare magnon gap to the renormalized value $\Delta_0 \to \Delta$.

The Lagrangian of a noninteracting spin-S impurity reads

$$\mathcal{L}_{\text{imp}} = i[\psi^\dagger(\boldsymbol{r},t)\partial_t \psi(\boldsymbol{r},t) - (\partial_t \psi^\dagger(\boldsymbol{r},t))\psi(\boldsymbol{r},t)]. \quad (3)$$

Here, ψ is the $2S+1$ component spinor. Hereafter, we set the energy of the noninteracting impurity to zero. The Lagrangian, which corresponds to the interaction between the impurity and the magnon field in the disordered phase, is [10]

$$\mathcal{L}_{\text{int}} = -\frac{\lambda}{S} \psi^\dagger (\boldsymbol{S} \cdot \boldsymbol{\phi}) \psi, \quad (4)$$

where λ is the coupling constant, $\boldsymbol{S} = (S_x, S_y, S_z)$ are the operators of the impurity's spin acting in the $(2S+1)$-dimensional Hilbert space.

The interaction of the impurity with magnons leads to appearance of a nonlocal part of spin density $\boldsymbol{s}(\boldsymbol{r})$. In order to find $\boldsymbol{s}(\boldsymbol{r})$, we use the Lagrangian of interaction of the system with an external magnetic field (see, e.g., Refs. [27]):

$$\mathcal{L}_B = -(\partial_t \boldsymbol{\phi} \cdot [\boldsymbol{B} \times \boldsymbol{\phi}]) + \frac{[\boldsymbol{B} \times \boldsymbol{\phi}]^2}{2} + \psi^\dagger (\boldsymbol{S} \cdot \boldsymbol{B}) \psi. \quad (5)$$

We have set here $\mu_B g = 1$. Note that Eq. (5) is still valid, if the magnetic field $\boldsymbol{B}$ is nonuniform. In contrast to the majority of previous works, where $\boldsymbol{B}$ is considered uniform, the nonuniformity of the probe magnetic field is crucial for the present paper. Linear in $\boldsymbol{B}$ terms in the Lagrangian (5) provide the following expression for the spin density:

$$\boldsymbol{s}(\boldsymbol{r}) = \left\langle \tfrac{1}{2}([\boldsymbol{\phi} \times \partial_t \boldsymbol{\phi}] + \text{H.c.}) + \psi^\dagger \boldsymbol{S} \psi \right\rangle = \boldsymbol{s}_{\text{nl}}(\boldsymbol{r}) + \boldsymbol{S}_{\text{imp}} \delta(\boldsymbol{r}). \quad (6)$$

The brackets $\langle \cdots \rangle$ denote an averaging over the ground state of the system. The term $1/2\langle[\boldsymbol{\phi} \times \partial_t \boldsymbol{\phi}] + \text{H.c.}\rangle$ in Eq. (6) is the nonlocal part of the spin density $\boldsymbol{s}_{\text{nl}}(\boldsymbol{r})$, induced by the impurity. The subscript "nl" stands hereafter for "nonlocal". The term $\langle \psi^\dagger \boldsymbol{S} \psi \rangle$ in Eq. (6) corresponds to the local spin $\boldsymbol{S}_{\text{imp}}$ at the impurity's site.

In addition to the spin density, we will consider the staggered magnetization, induced by the impurity. Writing down the Euler-Lagrange equation for the magnon field $\boldsymbol{\phi}$ from the action $\int dt d^3r \{\mathcal{L}_M + \mathcal{L}_{\text{int}}\}$ and taking the expectation value of the result, we obtain a Yukawa-like form of the staggered magnetization:

$$\langle \boldsymbol{\phi}(\boldsymbol{r}) \rangle = -\lambda \frac{e^{-\Delta r}}{4\pi r} \frac{\boldsymbol{S}_{\text{imp}}}{S}. \tag{7}$$

At the QCP, the exponent in Eq. (7) is close to unity and $\langle \phi(r) \rangle \propto 1/r$. Therefore, in order to find the corresponding prefactor, we only need to calculate the local spin at the impurity site, $\boldsymbol{S}_{\text{imp}}$.

To find the local as well as the nonlocal components of the impurity-induced spin density, we will proceed with the following procedure. We calculate the shift ϵ_B of the ground state energy, corresponding to the probe magnetic field $\boldsymbol{B}(\boldsymbol{r}') = \boldsymbol{B}\delta(\boldsymbol{r}' - \boldsymbol{r})$. The energy shift of the system reads $\epsilon_B = \boldsymbol{B} \cdot \boldsymbol{s}(\boldsymbol{r})$, therefore

$$\boldsymbol{s}(\boldsymbol{r}) = \left. \frac{\partial \epsilon_B}{\partial \boldsymbol{B}} \right|_{\boldsymbol{B}=0}. \tag{8}$$

The spin density $\boldsymbol{s}(\boldsymbol{r}) = \boldsymbol{e} s(r)$ and the staggered magnetization $\langle \boldsymbol{\phi}(\boldsymbol{r}) \rangle = \boldsymbol{e} \langle \phi(r) \rangle$ are directed along the impurity's spin $\boldsymbol{S}_{\text{imp}} = \boldsymbol{e} S_{\text{imp}}$ ($\boldsymbol{e}$ is a unit vector), and due to the spatial isotropy of the system, depend only on $r = |\boldsymbol{r}|$. The ground-state energy ϵ_g of the system is the position of the singularity of the retarded impurity's Green's function $\hat{G}_B(\epsilon)$ and can be found from the Dyson's equation

$$\hat{G}_B^{-1}(\epsilon) = \epsilon - \hat{\Sigma}(\epsilon) - B^\mu \hat{\Gamma}^\mu(\epsilon, r) = 0\,, \tag{9}$$

where $\hat{\Sigma}(\epsilon)$ is the self-energy of the impurity at zero magnetic field, $\hat{\Gamma}^\mu(\epsilon, r)$ is the vertex function, corresponding to the interaction of the system with the probe magnetic field. Note that in Eq. (9), we need to keep only the linear in B^μ terms. From rotational symmetry properties, the only possible "kinematic" structure of the vertex is

$$\hat{\Gamma}^\mu(\epsilon, r) = \Gamma(\epsilon, r) \hat{S}^\mu / S. \tag{10}$$

The vertex function can be split in local and nonlocal parts:

$$\hat{\Gamma}^\mu(\epsilon, r) = \begin{cases} \hat{\Gamma}^\mu_{\text{imp}}(\epsilon), & r = 0, \\ \hat{\Gamma}^\mu_{\text{nl}}(\epsilon, r), & r > 0. \end{cases} \tag{11}$$

Calculating the shift ϵ_B of the position of the singularity in the Green's function $\hat{G}_B(\epsilon)$ due to the probe magnetic field and using formula (8), we find the local and nonlocal components of spin density $s(r)$. Below, we will calculate the spin density using two approaches: the self-consistent Born approximation (for $S = 1/2$) and the renormalization group (for arbitrary S).

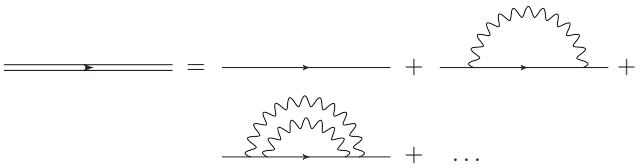

FIG. 2. Dyson's equation in SCBA. Double line is impurity's Green's function.

III. SELF-CONSISTENT BORN APPROXIMATION ($S = 1/2$)

The standard approach for the calculation of a single-fermion Green's function is the $1/N$ expansion for the O(N) group, where $N = 3$ is the number of magnon components. A summation of the leading terms in the $1/N$ expansion results in the self-consistent Born approximation (SCBA), see Fig. 2. We will apply SCBA to the case of $S = 1/2$ impurity only. As it will be demonstrated in Sec. IV C, for $S > 1/2$, corrections to the impurity-magnon vertex, which are disregarded in SCBA, become relevant. Therefore, in the latter case, SCBA fails and an application of the RG technique is necessary.

A. Impurity Green's function at zero magnetic field

To consider the interaction of the system with a probe magnetic field, we first calculate the Green's function of the impurity at zero magnetic field. The Green's function of the impurity at $\boldsymbol{B} = 0$ is proportional to the identity matrix in the spin space, $\hat{G}(\epsilon) = G(\epsilon)$. The Dyson's equation for the Green's function is graphically represented in Fig. 2. The analytical form of the equation reads

$$G(\epsilon) = \frac{1}{\epsilon - \Sigma(\epsilon) + i0}\,, \tag{12}$$

where the impurity self-energy is given by the following expression:

$$\begin{aligned} \hat{\Sigma}(\epsilon) &= \lambda^2 \int \frac{i d\omega}{2\pi} \sum_{\boldsymbol{q}} \sigma^\mu \hat{G}(\epsilon - \omega) D_{\mu\nu}(\omega, \boldsymbol{q}) \sigma^\nu \\ &= 3 \sum_{\boldsymbol{q}} M_{\boldsymbol{q}}^2 \hat{G}(\epsilon - \omega_{\boldsymbol{q}})\,. \end{aligned} \tag{13}$$

Here, $\omega_{\boldsymbol{q}} = \sqrt{\Delta^2 + \boldsymbol{q}^2}$ is the magnon dispersion, $M_{\boldsymbol{q}} = \lambda/\sqrt{2\omega_{\boldsymbol{q}}}$ is the matrix element corresponding to the emission of a magnon with momentum $\boldsymbol{q}$ by the impurity, and $D_{\mu\nu}(\omega, \boldsymbol{q}) = \delta_{\mu\nu}/(\omega^2 - \omega_{\boldsymbol{q}}^2 + i0)$ is the magnon propagator. We expressed the spin-1/2 operators via Pauli matrices $S^\mu = \sigma^\mu/2$. The combinatorial factor 3 in Eq. (13) comes from a summation over the intermediate polarization states of the magnon.

The sum over momentum $\boldsymbol{q}$ in Eq. (13) diverges at large $|\boldsymbol{q}|$, therefore we have to introduce an ultraviolet cutoff Λ. The parameter Λ depends on a particular realization of the system and can be estimated as the inverse lattice spacing in the host AF.

The solution to Dyson's equation (12) near the QCP ($\Delta \to 0$) has the following form:

$$G^{-1}(\epsilon) = (\epsilon - \epsilon_0 + i0) \sqrt{1 + \frac{3\lambda^2}{2\pi^2} \ln\left(\frac{\Lambda}{\epsilon_0 + \Delta - \epsilon - i0}\right)}. \tag{14}$$

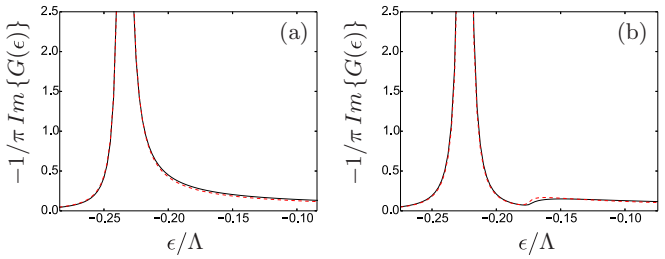

FIG. 3. (Color online) Spectral function of an $S = 1/2$ impurity obtained in SCBA. (a) corresponds to the QCP ($\Delta = 0$) and (b) corresponds to a magnon gap $\Delta = 0.05\Lambda$. The effective coupling constant is set to $\kappa = 0.6$. The solid black line corresponds to the Green's function, calculated numerically, the red dashed line corresponds to analytical formula (14). Note that in (a), the position of the pole and the branching point are merging.

In the vicinity of the singularity point $\epsilon_0 \approx -3\Lambda\lambda^2/4\pi^2$. Formula (14) is obtained with logarithmic accuracy, i.e., assuming that $\ln(\frac{\Lambda}{\epsilon_0+\Delta-\epsilon}) \gg 1$.

The Green's function (14) has a nontrivial analytic structure. At finite magnon gaps, the quasiparticle pole at $\epsilon = \epsilon_0$ is separated by the gap Δ from the incoherent part of the Green's function. At the QCP, when $\Delta \to 0$, the pole and the branching point singularity are merging. The quasiparticle residue of the impurity Green's function $G(\epsilon)$ vanishes in the vicinity of the QCP:

$$Z = \left(1 - \frac{\partial\Sigma(\epsilon_0)}{\partial\epsilon}\right)^{-1} = \left.\frac{1}{\sqrt{1 + \frac{3\lambda^2}{2\pi^2}\ln\left(\frac{\Lambda}{\Delta}\right)}}\right|_{\Delta\to 0} \to 0. \quad (15)$$

Vanishing quasiparticle residue is the first signal of delocalization of the impurity-induced spin cloud and therefore is an indication of SCS [23].

The typical value of the impurity-magnon coupling constant λ can be estimated from the lattice model, shown in Fig. 1. Lattice calculations [28] on the basis of bond-operator mean-field theory result in the value of the effective coupling constant $\kappa = 3\lambda^2/2\pi^2 \sim 0.5$, appearing in front of the logarithm in formula (14). Therefore the logarithmic corrections are significant in the vicinity of the QCP.

The analytical result (14) for the impurity Green's function can be compared with the direct numerical solution of Dyson's equation (12), the corresponding plots for spectral functions $-1/\pi\ \mathrm{Im}\{G(\epsilon)\}$ are plotted in Fig. 3. An artificial broadening $i0 \to i2.5 \times 10^{-3}\Lambda$ is introduced in the numerical procedure and in analytical formula (14). We see an excellent agreement between the numerical and the analytical results.

Let us make a comment about the validity domain of SCBA for the results in the present section, and all following results, which will be derived in Secs. III B and III C. Formally, SCBA relies only on a $1/N$ expansion of the O(N) group, independent of the value of the coupling constant λ. SCBA is applicable for arbitrary λ, in contrast to the RG method, which works only for small λ. We will return to this discussion later, in Sec. IV A.

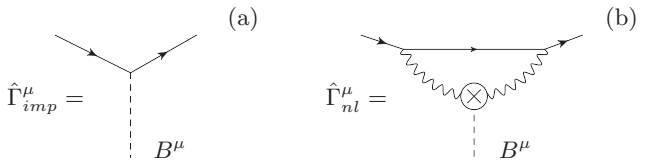

FIG. 4. Example of diagrams for a coupling between a probe magnetic field $\boldsymbol{B}$ and (a) an impurity spin or (b) the nonlocal spin density. The solid line corresponds to a bare ($\lambda = 0$) impurity Green's function, the wavy line represents magnons, and the dashed line represents the probe magnetic field $\boldsymbol{B}$. The cross on the magnon line corresponds to the magnon-$\boldsymbol{B}$ vertex, provided by the term $\boldsymbol{B}[\boldsymbol{\phi} \times \dot{\boldsymbol{\phi}}]$ in the Lagrangian (5).

B. Calculation of nonlocal spin density $s_{\mathrm{nl}}(r)$

To evaluate the nonlocal spin density induced by the impurity at distances $r > 0$, we substitute the Green's function pole position $\epsilon_g = \epsilon_0 + \epsilon_B$ into Eq. (9), expand it in ϵ_B up to the first order, and use Eq. (8). The result reads

$$s_{\mathrm{nl}}(r) = Z\Gamma_{\mathrm{nl}}(\epsilon_0, r)\,. \quad (16)$$

The leading in coupling constant λ contribution to the vertex $\hat{\Gamma}^{\mu}_{\mathrm{nl}}$ is represented by the Feynman diagram shown in Fig. 4(b). The analytical expression for the diagram is the following:

$$\begin{aligned}\hat{\Gamma}^{\mu}_{\mathrm{nl}}(\epsilon, r) &= \Gamma_{\mathrm{nl}}(\epsilon, r)\sigma^{\mu} \\ &= \int \frac{i d\omega}{2\pi} \sum_{\boldsymbol{q},\boldsymbol{k}} (\lambda\sigma^{\varkappa})\hat{G}_0(\epsilon - \omega)(\lambda\sigma^{\beta}) \\ &\quad \times D_{\varkappa\nu}(\omega, \boldsymbol{k})[-2i\omega\,\varepsilon_{\mu\nu\alpha}\, e^{i(\boldsymbol{q}-\boldsymbol{k})\boldsymbol{r}}]D_{\beta\alpha}(\omega, \boldsymbol{q})\,, \quad (17)\end{aligned}$$

where $\hat{G}_0(\epsilon) = 1/(\epsilon + i0)$ is the bare retarded Green's function of a noninteracting impurity. The expression in square brackets corresponds to the magnon-probe magnetic field vertex, which we show in Fig. 4(b) as a circle with a cross inside.

The SCBA equation for the vertex $\hat{\Gamma}^{\mu}_{\mathrm{nl}}(\epsilon, r)$ is graphically represented in Fig. 5. The analytical form of the equation for the vertex is

$$\Gamma_{\mathrm{nl}}(\epsilon, r) = \Gamma^{(0)}_{\mathrm{nl}}(\epsilon, r) - \sum_{\boldsymbol{q}} M_q^2 G^2(\epsilon - \omega_q)\Gamma_{\mathrm{nl}}(\epsilon - \omega_q, r), \quad (18)$$

where $\Gamma^{(0)}_{\mathrm{nl}}(\epsilon, r)$ corresponds to the first term in the right-hand side (rhs) of the diagrammatic equation in Fig. 5 and reads

$$\Gamma^{(0)}_{\mathrm{nl}}(\epsilon, r) = 2\lambda^2 \sum_{\boldsymbol{q},\boldsymbol{k}} e^{i(\boldsymbol{q}-\boldsymbol{k})\boldsymbol{r}} \frac{G(\epsilon - \omega_q) - G(\epsilon - \omega_k)}{\omega_q^2 - \omega_k^2}\,. \quad (19)$$

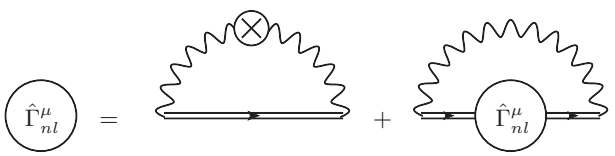

FIG. 5. Diagrammatic equation for "nonlocal" vertex function $\hat{\Gamma}^{\mu}_{\mathrm{nl}}$.

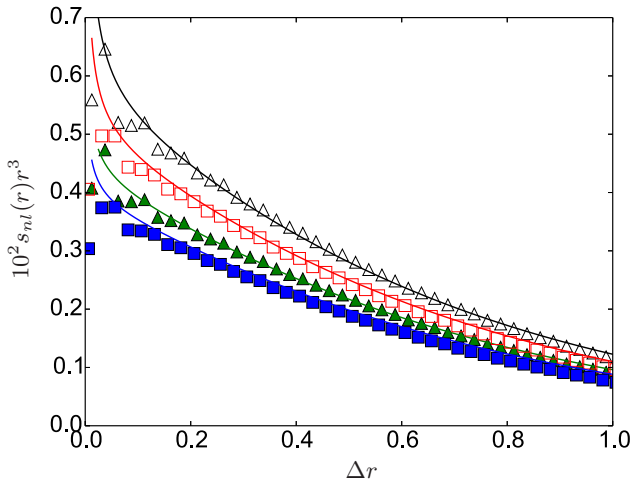

FIG. 6. (Color online) Spin density $s_{\rm nl}(r)$ (multiplied by r^3) induced by an $S = 1/2$ impurity as a function of the dimensionless distance $y = \Delta r$ calculated in SCBA. Points represent numerical results for different values of magnon gap and effective coupling constant $\kappa = 3\lambda^2/2\pi^2$. Squares correspond to $\Delta = 6.25 \times 10^{-3}\Lambda$, triangles correspond to $\Delta = 1.25 \times 10^{-2}\Lambda$; filled markers represent $\kappa = 0.3$, open markers correspond to $\kappa = 0.6$. The solid line is the analytical approximation (20).

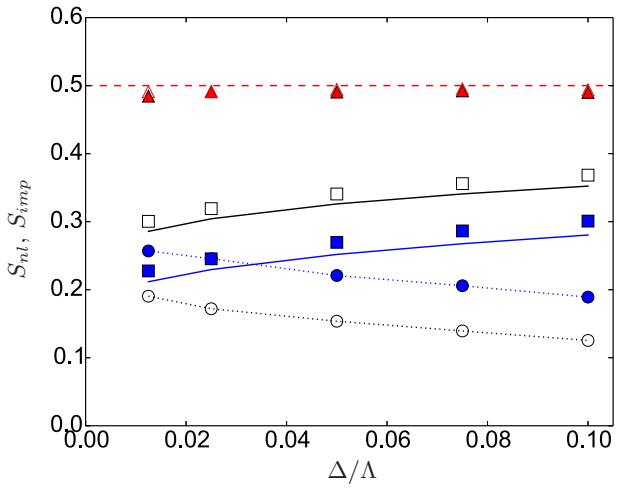

FIG. 7. (Color online) Integral nonlocal spin $S_{\rm nl}$ and local spin of the imputity $S_{\rm imp}$ as a function of the magnon gap Δ in SCBA. Full and open markers correspond respectively to the following values of the effective coupling constant: $\kappa = 0.6$ and $\kappa = 0.3$. Circles correspond to $S_{\rm nl}$, squares represent $S_{\rm imp}$, and triangles show the net spin $S_{\rm nl} + S_{\rm imp}$. The solid lines are theoretical predictions for the local impurity spin $S_{\rm imp}$, given by Eq. (25). The dotted lines are visual guides for $S_{\rm nl}$. The red dashed line corresponds to the net spin equal to $1/2$.

To obtain expressions (18) and (19), we performed an integration over ω in the rhs of the original SCBA equation, shown in Fig. 5. The factor (-1) in Eq. (18) comes from the algebraic identity for the Pauli matrices $\sigma^\mu\sigma^\nu\sigma^\mu = -\sigma^\nu$. Formula (19) follows from (17), where the bare impurity Green's function is changed to the "dressed" Green's function $G(\epsilon)$, shown in Fig. 2.

To find $s_{\rm nl}(r)$, we solve numerically Eq. (18) for the vertex $\Gamma_{\rm nl}(\epsilon,r)$ and substitute the result together with the quasiparticle residue Z, obtained from a numerical solution of Dyson's equation (12), to Eq. (16). A solution to Eq. (18) has been found iteratively, starting iterations from the $\Gamma_{\rm nl}(\epsilon,r) = \Gamma^{(0)}_{\rm nl}(\epsilon,r)$. The results of the calculation of the spin density $s_{\rm nl}(r)$ for different values of the magnon gap Δ and coupling constant λ are presented in Fig. 6.

For the purpose of computational efficiency, we use a spherical cutoff $|\boldsymbol{q}|,|\boldsymbol{k}| \leqslant \Lambda$ in integrals in Eqs. (18) and (19), instead of integrating over a cubic Brillouin zone. This cutoff scheme results in the appearance of significant r oscillations in the induced spin density $s_{\rm nl}(r)$, where the period of oscillations is $r \sim 1/\Lambda$ and the amplitude of the oscillations is decaying with increasing r. It is clear that these oscillations are byproducts of the rigid spherical cutoff and will be notably suppressed, if one performs a proper 3D integration over the cubic Brillouin zone. Hence, in Fig. 6, we plot numerical data for the spin-density, averaged over the period of the oscillations.

Our numerical calculations show that the starting approximation $\Gamma^{(0)}_{\rm nl}(\epsilon,r)$ for the vertex function and the solution $\Gamma_{\rm nl}(\epsilon,r)$ of the SCBA equation (18) are very close to each other. Therefore, to obtain an analytical approximation for the nonlocal spin density, we substitute (19) in Eq. (16) and use formula (14) for the impurity's Green's function, the result reads

$$s_{\rm nl}(r) = \frac{\lambda^2\Delta}{4\pi^3\sqrt{1+\frac{3\lambda^2}{2\pi^2}\ln\frac{\Lambda}{\Delta}}\sqrt{1+\frac{3\lambda^2}{2\pi^2}\ln\Lambda r}}\frac{K_1(2\Delta r)}{r^2}. \quad (20)$$

Here, $K_1(x)$ is the Macdonald function of the first kind. At distances $1/\Lambda < r < 1/\Delta$, using an expansion of the Macdonald function $K_1(x) \to 1/x$ at $x \to 0$, we obtain a power-law asymptotics for the spin density with logarithmic corrections:

$$s_{\rm nl}(r) \to \frac{\lambda^2}{8\pi^3 r^3}\frac{1}{\sqrt{\left(1+\frac{3\lambda^2}{2\pi^2}\ln\frac{\Lambda}{\Delta}\right)\left(1+\frac{3\lambda^2}{2\pi^2}\ln\Lambda r\right)}}. \quad (21)$$

At large distances $r > 1/\Delta$, the spin density (20) is exponentially suppressed: $s_{\rm nl}(r) \propto e^{-2\Delta r}/r^{5/2}$. In Fig. 6, solid lines correspond to the analytical result given by Eq. (20). One can see an excellent agreement between the analytical and the numerical results.

The net spin of the system, which is given by the sum of the local impurity spin and the spin of the nonlocal cloud, is conserved and must be equal to $S = 1/2$. The integral spin, corresponding to the nonlocal spin density

$$S_{\rm nl} = \int d^3r s_{\rm nl}(r), \quad (22)$$

is plotted in Fig. 7 versus Δ/Λ. We use the numerical results for $s_{\rm nl}(r)$, shown in Fig. 6, in order to obtain $S_{\rm nl}$. One can see that the nonlocal spin $S_{\rm nl}$ logarithmically increases with decreasing Δ and tends to $S_{\rm nl} = 1/2$ at the critical point. Therefore the rest of the spin should be attributed to the impurity's spin $S_{\rm imp} = 1/2 - S_{\rm nl}$, which vanishes at the QCP. We check this statement in Sec. III C by calculating the local spin of the impurity.

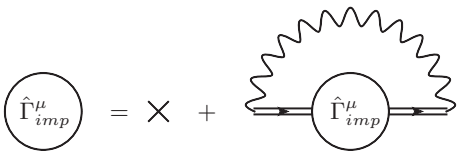

FIG. 8. Diagrammatic equation for "local" vertex function $\hat{\Gamma}^{\mu}_{\rm imp}$. Cross represents bare vertex $\Gamma^{(0)}_{\rm imp} = 1$.

C. Local spin of the impurity and staggered magnetization

To calculate the impurity spin, localized at $\boldsymbol{r} = 0$, we use a similar approach to that we used in the previous section. We introduce a local magnetic field $\boldsymbol{B}(\boldsymbol{r}) = \boldsymbol{B}\delta(\boldsymbol{r})$ and calculate the energy shift of the impurity due to the magnetic field. The result for the impurity spin reads

$$S_{\rm imp} = \frac{Z}{2}\Gamma_{\rm imp}(\epsilon)\Big|_{\epsilon=\epsilon_0}. \tag{23}$$

A diagrammatic equation for the vertex function $\hat{\Gamma}^{\mu}_{\rm imp}(\epsilon) = \Gamma_{\rm imp}(\epsilon)\sigma^{\mu}$ in SCBA has the graphical representation shown in Fig. 8.

The corresponding analytical form of the equation, represented in Fig. 8, is

$$\Gamma_{\rm imp}(\epsilon) = 1 - \sum_{\boldsymbol{q}} M^2_{\boldsymbol{q}} G^2(\epsilon - \omega_{\boldsymbol{q}})\Gamma_{\rm imp}(\epsilon - \omega_{\boldsymbol{q}}). \tag{24}$$

Solving equation (24) and substituting the solution into Eq. (23), we obtain the spin of the impurity with logarithmic accuracy:

$$S_{\rm imp} = \frac{1}{2\left(1 + \frac{3\lambda^2}{2\pi^2}\ln\frac{\Lambda}{\Delta}\right)^{2/3}}. \tag{25}$$

We also calculate the residual spin of the impurity numerically, solving iteratively Eq. (24). Both analytical and numerical results for $S_{\rm imp}$ at different values of the parameters Δ and λ are plotted in Fig. 7. We see good agreement between the analytical and the numerical results. From Fig. 7, we can notice that the impurity spin logarithmically tends to zero when we approach to the QCP, $\Delta \to 0$. In Fig. 7, we also show the net spin $S_{\rm imp} + S_{\rm nl}$ for different values of Δ and λ.

The results of our calculations, presented in Eqs. (21) and (25) and also in Figs. 6 and 7, show that at the QCP the local spin is approaching to zero and the spin of the system is accumulated in the nonlocal spin cloud. This delocalized spin cloud around impurity has a size proportional to the inverse magnon gap $r \simeq 1/\Delta$, and therefore a significant part of the impurity spin is separated from the charge, localized at $r = 0$. We will return to this discussion again in Sec. IV B.

The net spin of the system equals to 1/2. This is the exact statement and can be demonstrated at the diagrammatic level. One can trace mutual cancellations of corrections to the impurity spin and integral spin of the nonlocal cloud in every order in λ. Corrections to the impurity spin $S_{\rm imp}$ are canceled by corrections to the integral spin $S_{\rm nl}$. The numerical results for the net spin of the system presented in Fig. 7 are consistent with the conservation of spin.

Using Eqs. (7) and (25), we obtain the following expression for the staggered magnetization induced by the spin-1/2 impurity:

$$\langle\phi(r)\rangle = -\lambda\frac{e^{-\Delta r}}{4\pi r}\frac{1}{\left(1 + \frac{3\lambda^2}{2\pi^2}\ln\frac{\Lambda}{\Delta}\right)^{2/3}}. \tag{26}$$

Away from the QCP, the staggered magnetization, induced by the impurity is exponentially small. In the vicinity of the QCP, the prefactor in Eq. (26) becomes logarithmically suppressed, however, the staggered magnetization decays only as $\langle\phi(r)\rangle \propto 1/r$.

IV. RENORMALIZATION GROUP APPROACH IN (3+1)D

In this section, we calculate the nonlocal and local components of the spin density using the RG technique in $3+1$ dimensions. In the RG approach, the coupling constant λ becomes dependent on the energy scale. Since $(3+1)$D is the upper critical dimension, the evolution of the running coupling constant is logarithmic. It leads to logarithmic corrections to $s_{\rm nl}$ and $\langle\phi(r)\rangle$, similar to results (21) and (26) obtained in SCBA. We derive our results for the case of an arbitrary spin S of the impurity in Secs. IV A and IV B, and then we analyze the limit of a large spin S in Sec. IV C.

In the RG technique, we consider the evolution of the coupling constant λ, quasiparticle residue Z, spin density, and staggered magnetization with the energy scale μ, starting evolution from the ultraviolet scale Λ and finishing at the infrared scale Δ. The scale μ here has the meaning of the characteristic energy transfer from magnons to the impurity. At the ultraviolet scale Λ, we set the parameters of the theory to the bare values; in our calculations, Λ plays the role of a renormalization point. Observables in the vicinity of the QCP are calculated as a result of the RG evolution from the ultraviolet scale Λ to the infrared scale $\mu = \Delta$.

A. Evolution of the coupling constant and quasiparticle residue

First, we calculate the evolution of the coupling constant $\lambda(\mu)$. The one-loop correction to the coupling constant is represented by the sum of diagrams shown in Fig. 9.

Note that in the RG approach, the correction to the coupling constant includes the vertex correction [Fig. 9(b)], and also the self-energy correction [Fig. 9(c)]. This is different from SCBA, in which we disregard diagram (b).

The contribution $\delta\lambda^{(b)}$ to the coupling constant correction is given by the diagram (b) in Fig. 9 and reads

$$\begin{aligned}\boldsymbol{S}^{\mu}\delta\lambda^{(b)} &= \lambda^3\frac{\boldsymbol{S}^{\nu}\boldsymbol{S}^{\mu}\boldsymbol{S}^{\nu}}{S^2}\int\frac{id\omega'}{2\pi}\sum_{\boldsymbol{k}}G_0(\mu-\omega')\\ &\times G_0(\mu-\omega-\omega')D(\omega',\boldsymbol{k})\\ &\approx \boldsymbol{S}^{\mu}\frac{(S(S+1)-1)}{S^2}\frac{\lambda^3}{4\pi^2}\ln\frac{\Lambda}{\mu}.\end{aligned} \tag{27}$$

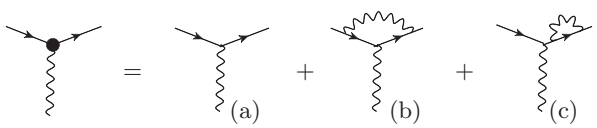

FIG. 9. One-loop corrections to the impurity-magnon coupling constant λ.

After canceling out the factor $\boldsymbol{S}^{\mu}$ from both sides of Eq. (27), we obtain $\delta\lambda^{(b)}$. The second contribution $\delta\lambda^{(c)}$, which comes from the diagram (c) in Fig. 9 reads

$$\delta\lambda^{(c)} = \lambda^3\left(1+\frac{1}{S}\right)G_0(\mu-\omega) \times \int \frac{i d\omega'}{2\pi}\sum_{\boldsymbol{k}} G_0(\mu-\omega-\omega')D(\omega',\boldsymbol{k}) \quad (28)$$

and contains linear in Λ and logarithmic in Λ terms. The linear term corresponds to the shift of the position of the quasiparticle pole ϵ_0 in the impurity's Green's function and therefore is irrelevant for our purposes. The logarithmic term in $\delta\lambda^{(2)}$ reads

$$\delta\lambda^{(c)} \to -\frac{\lambda^3}{4\pi^2}\left(1+\frac{1}{S}\right)\ln\frac{\Lambda}{\mu}. \quad (29)$$

The total correction to the coupling constant λ is

$$\delta\lambda = \delta\lambda^{(b)} + \delta\lambda^{(c)} = -\frac{\lambda^3}{4S^2\pi^2}\ln\frac{\Lambda}{\mu}. \quad (30)$$

Note that for $S = 1/2$ the vertex correction (27) is suppressed by the factor $1/N = 1/3$, comparing to $\delta\lambda^{(c)}$. This suppression corresponds to the standard $1/N$ expansion of O(N) group. However, at large S, the $1/N$ suppression of $\delta\lambda^{(b)}$ is compensated by S, and hence $\delta\lambda^{(b)}$ and $\delta\lambda^{(c)}$ to a large extent compensate each other, $\delta\lambda^{(b)} \approx -\delta\lambda^{(c)}$. Thus, at large S, the vertex correction becomes significant and can not be disregarded. This is the reason why SCBA fails in the case of large impurity spin.

In the paradigm of RG, the evolution of the physical parameters on some energy scale μ is determined by the value of $\lambda(\mu)$ on the same scale. Hence Eq. (30) results in the following Gellman-Low equation:

$$\frac{d\lambda(\mu)}{d\ln\mu} = \frac{\lambda^3(\mu)}{4S^2\pi^2}. \quad (31)$$

The solution to Eq. (31) with the initial condition $\lambda(\Lambda) = \lambda$ is

$$\lambda(\mu) = \frac{\lambda}{\sqrt{1+\frac{\lambda^2}{2S^2\pi^2}\ln\frac{\Lambda}{\mu}}}. \quad (32)$$

Note that the running coupling constant (32) vanishes in the infrared limit: $\lambda(\mu) \to 0$ at $\mu \simeq \Delta \to 0$. The RG scale μ is bounded from below by the value of the magnon gap $\mu \geqslant \Delta$.

In order to find the quasiparticle residue of the impurity Green's function, we consider a one-loop correction to the impurity's self-energy. The logarithmic part of this correction was already calculated as a part of the diagram (c) in Fig. 9. The corresponding equation for the evolution of $Z(\mu)$ reads

$$\frac{d\ln Z(\mu)}{d\ln\mu} = \left(1+\frac{1}{S}\right)\frac{\lambda^2(\mu)}{4\pi^2}. \quad (33)$$

The solution to Eq. (33) with an initial condition $Z(\Lambda) = 1$ reads

$$Z(\mu) = \frac{1}{\left(1+\frac{\lambda^2}{2S^2\pi^2}\ln\frac{\Lambda}{\mu}\right)^{S(S+1)/2}} = \left(\frac{\lambda(\mu)}{\lambda}\right)^{S(S+1)}. \quad (34)$$

The quasiparticle residue $Z(\mu)$ vanishes, while approaching to the QCP: $\mu \simeq \Delta \to 0$.

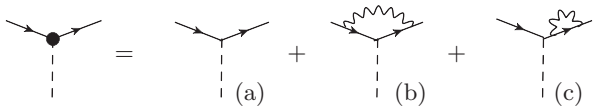

FIG. 10. One-loop corrections to "local" spin S_{imp}.

Note that the RG approach, being used in the current section, is valid if the effective coupling constant $\tilde{\kappa} = \lambda^2/2S^2\pi^2 < 1$, since we perform a perturbative expansion, such as in Eq. (30). However, the proper expansion parameter in the vicinity of the QCP is not $\tilde{\kappa}$, but $\tilde{\kappa}\ln\Lambda/\Delta$. The RG method (in the single-loop approximation) allows to sum up (leading) logarithmic corrections of the following kind: $\tilde{\kappa}^m\sum_n \tilde{\kappa}^n \ln^n(\Lambda/\Delta)$. Therefore the results obtained within the one-loop RG in Sec. IV are valid when $\tilde{\kappa} < 1$ and $\tilde{\kappa}^2\ln(\Lambda/\Delta) < 1$, but the product $\tilde{\kappa}\ln(\Lambda/\Delta)$ can have an arbitrary value.

B. Impurity spin and nonlocal spin density

Now we consider the RG evolution of the impurity spin S_{imp} and spin density distribution $s(r)$ with the renormalization scale μ. As in Sec. III, we calculate S_{imp} and $s(r)$, considering the interaction of the system with a probe magnetic field $\boldsymbol{B}(\boldsymbol{r})$.

We start from a calculation of the corrections to S_{imp} due to the interaction of the impurity with magnons. One-loop corrections to S_{imp} are shown in Fig. 10.

Note that the diagrams in Fig. 10 are analogous to the diagrams in Fig. 9 for corrections to the coupling constant λ. The only difference is that the impurity-magnetic field coupling $\boldsymbol{S}_{\text{imp}}\cdot\boldsymbol{B}$ is proportional to the impurity spin $\boldsymbol{S}_{\text{imp}}$. Hence, the RG evolution equation reads

$$\frac{dS_{\text{imp}}(\mu)}{d\ln\mu} = \frac{\lambda^2(\mu)}{4S^2\pi^2}S_{\text{imp}}(\mu). \quad (35)$$

The solution to Eq. (35) with the initial condition $S_{\text{imp}}(\Lambda) = S$ is

$$S_{\text{imp}}(\mu) = \frac{S}{\sqrt{1+\frac{\lambda^2}{2S^2\pi^2}\ln\frac{\Lambda}{\mu}}}, \quad (36)$$

which is proportional to solution (32) for the running coupling $\lambda(\mu)$. The local spin at the impurity site is equal to $S_{\text{imp}}(\mu \simeq \Delta)$ and approaches to zero at the QCP. Using the result (36) and relation (7), we obtain the distribution of the staggered magnetization around an impurity:

$$\langle\phi(r)\rangle = -\frac{\lambda}{4\pi r}\frac{e^{-\Delta r}}{\sqrt{1+\frac{\lambda^2}{2S^2\pi^2}\ln\frac{\Lambda}{\Delta}}}. \quad (37)$$

Now we calculate the nonlocal spin density $s_{\text{nl}}(r)$. In the RG technique, it is more natural to use the momentum representation for the spin density, therefore we write the evolution equation for the Fourier component $s_{\text{nl}}(q)$. Leading in λ^2 contributions to $s_{\text{nl}}(q)$ are provided by the one-loop diagram shown in Fig. 4(b). Evaluation of this diagram with logarithmic precision leads to

$$s_{\text{nl}}^{(0)}(q) \approx \begin{cases} \frac{\lambda^2}{4S\pi^2}\ln\frac{\Lambda}{\mu}, & \mu \gg q, \\ \frac{\lambda^2}{4S\pi^2}\ln\frac{\Lambda}{q}, & \mu \ll q. \end{cases} \quad (38)$$

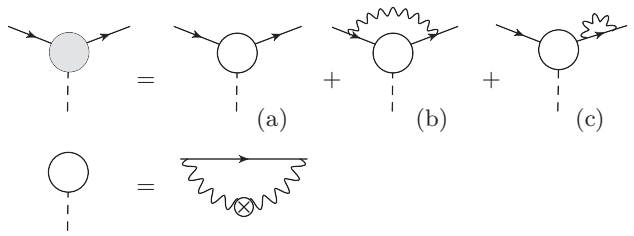

FIG. 11. One-loop corrections to the nonlocal spin density $s_{\rm nl}(q)$.

Fourier transform of the second line of Eq. (38) gives the spin density $s_{\rm nl}^{(0)}(r) = \lambda^2/16S\pi^3 r^3$ at the distances $1/\Lambda < r < 1/\Delta$. In analogy with the result (21), obtained in SCBA, in RG calculations, we should expect logarithmic corrections to $\propto 1/r^3$ distribution. Note that the logarithmic corrections are important, because they provide a proper normalization condition of the integral nonlocal spin $\int d^3r s_{\rm nl}(r) \to S$ at the QCP. The volume integral of the spin density $\propto 1/r^3$ is logarithmically divergent, $\propto \ln \Lambda/\Delta$, if we disregard the log corrections.

In order to account for the RG evolution of the spin-density, we evaluate the single-loop corrections to the leading diagram presented in Fig. 4(b). Diagrams (b) and (c) in Fig. 11 represent these corrections, which are similar to the corresponding diagrams in Figs. 9 and 10.

The RG evolution of the nonlocal spin density distribution reads

$$\frac{ds_{\rm nl}(q,\mu)}{d\ln\mu} = \begin{cases} \frac{\lambda^2(\mu)}{4S^2\pi^2} s_{\rm nl}(q,\mu) - \frac{\lambda^2(\mu)}{4S\pi^2}, & \mu \gg q, \\ \frac{\lambda^2(\mu)}{4S^2\pi^2} s_{\rm nl}(q,\mu), & \mu \ll q. \end{cases} \tag{39}$$

Note that the equation for the evolution of the spin density with μ is different in two domains, $\mu \gg q$ and $\mu \ll q$, which is due to the fact that the one-loop expression (38) for the spin density has different forms in both domains. We solve Eq. (39) separately in the two domains and match the solutions at $\mu \simeq q$. As an initial condition for the evolution equation (39), we set $s_{\rm nl}(\Lambda) = 0$. We obtain the following result for the spin density at infrared scale $\mu \simeq \Delta$:

$$s_{\rm nl}(q) = \frac{S}{\sqrt{1 + \frac{\lambda^2}{2S^2\pi^2}\ln\frac{\Lambda}{\Delta}}} \left(\sqrt{1 + \frac{\lambda^2}{2S^2\pi^2}\ln\frac{\Lambda}{q}} - 1 \right). \tag{40}$$

The condition of the net spin conservation in the momentum representation has the form $s_{\rm nl}(q)|_{q\to 0} + S_{\rm imp} = S$. Using expressions (36) and (40), it is easy to check the net spin conservation, having in mind that the low bound for the momentum q in our formulas is $q \simeq \Delta$.

Calculating the Fourier transform of Eq. (40), we obtain the spatial distribution of the induced spin density:

$$s_{\rm nl}(r) = \frac{\lambda^2}{16S\pi^3 r^3 \sqrt{1 + \frac{\lambda^2}{2S^2\pi^2}\ln\frac{\Lambda}{\Delta}} \sqrt{1 + \frac{\lambda^2}{2S^2\pi^2}\ln\Lambda r}} \tag{41}$$

at distances $1/\Lambda < r < 1/\Delta$. Using (41) and (36), one can verify the conservation of the net spin in r representation: $\int d^3r\, s_{\rm nl}(r) + S_{\rm imp} = S$. The integration of the nonlocal spin density should be performed in the range of distances $1/\Lambda < r < 1/\Delta$, which is defined by the infrared and the ultraviolet cutoffs of our theory.

Note that at the QCP, the main contribution to the nonlocal spin $\int d^3r\, s_{\rm nl}(r)$ comes from large distances $r < 1/\Delta \to \infty$. Indeed, the integral

$$\int_{1/\Lambda \leqslant r \leqslant R} d^3r\, s_{\rm nl}(r) = S \frac{\sqrt{1 + \frac{\lambda^2}{2S^2\pi^2}\ln\Lambda R} - 1}{\sqrt{1 + \frac{\lambda^2}{2S^2\pi^2}\ln\frac{\Lambda}{\Delta}}} \tag{42}$$

logarithmically grows as a function of the upper integration limit R, which means that a major part of spin in the nonlocal cloud is accumulated at distances of the order of $R \simeq 1/\Delta$. At the same time, the local spin of the impurity $S_{\rm imp}$ vanishes at the QCP, see Eq. (36). Therefore we conclude that at the QCP the impurity spin is spatially separated from the impurity charge.

The results (34), (37), and (41) obtained in RG technique are similar to corresponding answers (15), (26), and (21) obtained in SCBA. For the spin $S = 1/2$, the difference is in the numerical factors in front of the logarithms: $3\lambda^2/2\pi^2$ in SCBA, comparing to $2\lambda^2/\pi^2$ in RG. For Z and $\langle\phi(r)\rangle$, the powers of the logarithms are also insignificantly changed: $1/2 \to 3/8$ and $2/3 \to 1/2$, respectively. The reason for these minor changes is the $1/N$ vertex correction, which is accounted in the RG approach [see diagram (b) in Fig. 9], and is disregarded in SCBA. The RG results are more accurate than the SCBA results. However, the expansion of the RG results and the SCBA results coincide up to the single-loop order (first order in λ^2).

Our results show that in a three-dimensional antiferromagnet, the impurity-induced spin density at the QCP decays as $s_{\rm nl}(r) \propto 1/r^3$ [with corresponding $\ln(r)$ corrections] and the staggered magnetization decays as $\langle\phi(r)\rangle \propto 1/r$. The RG flow in $(3+1)$D leads only to $\ln(r)$ corrections to $s_{\rm nl}(r)$, leaving the power laws unchanged.

On the other hand, in $(2+1)$D, the RG flow has Wilson-Fisher fixed points, which instead of logarithmic corrections provide nontrivial critical exponents for the correlation functions. For instance, the impurity quasiparticle residue $Z \propto \Delta^{\eta'/2}$ (see, e.g., Refs. [10,29]) acquires an anomalous dimension near the QCP, $\eta' = 1$ (in the one-loop approximation). It results in the following scaling law [10] in the spin density distribution $s_{\rm nl}(r) \propto 1/r^{2-\eta'/2} \approx 1/r^{3/2}$. A more accurate value of the anomalous dimension $\eta' \approx 0.4$ is known from a quantum Monte Carlo study [11] of hole-induced magnetization in a Heisenberg bilayer model. Following similar arguments to the ones used to obtain Eq. (7), the staggered magnetization in $(2+1)$D reads [10] $\langle\phi(r)\rangle \propto \Delta^{\eta'/2}\ln(\Delta r)$ at $\Delta r \ll 1$. Although the scaling laws are well known, the problem of calculation of the corresponding prefactors still remains unsolved.

As one can see, the integral spin $\int^R d^2r s_{\rm nl}(r)$ accumulated in the nonlocal cloud in $(2+1)$D grows as a power law of the upper integration limit $\propto R^{\eta'/2}$, in contrast with the slow logarithmic growth in $(3+1)$D [see Eq. (42)]. Therefore the effect of spatial spin-charge separation at the QCP is more pronounced in two-dimensional systems, rather then in three-dimensional systems.

So far, we have considered the physics of spin-charge separation when approaching the QCP from the disordered phase. What happens when approaching the QCP from the AF ordered Neel phase? In the ordered phase, the interaction of an impurity (hole) with a probe magnetic field cannot be written as $\psi^\dagger(\boldsymbol{S}\cdot\boldsymbol{B})\psi$ since both the impurity and the antiferromagnetic background interact with the magnetic field. The interaction Lagrangian, instead, has quite an unusual form [30,31]:

$$\delta\mathcal{L}_B = (\boldsymbol{B}\cdot\boldsymbol{n})\,\psi^\dagger(\boldsymbol{S}\cdot\boldsymbol{n})\psi, \tag{43}$$

where $\boldsymbol{n}(\boldsymbol{r})$ is the Neel ordering vector, $\boldsymbol{n}^2 = 1$. The interaction energy (43) of the impurity with a probe magnetic field depends on the direction of the spontaneous staggered magnetization $\boldsymbol{n}$. This implies that the notion of an impurity spin in the phase with broken rotational invariance is not well defined. This is why usually people use the notion of a pseudospin originating from two AF sublattices. For example, a holon carries charge and a psedospin, but it does not carry spin in the usual sense. Therefore it is possible to say that deeply in the Neel phase, the impurity spin and charge are always separated, or more precisely, partially separated, see also the discussion in Ref. [32].

Even though the notion of the impurity spin in the AF phase is poorly defined, it is not meaningless to ask a question about the distribution of the induced magnetization around the impurity. We do not have a complete solution to this problem, but rather propose an intuitive physical picture. Interestingly, this problem has direct relevance to the transition to the Adler's theorem regime in the ordered phase. By analogy with the case of 2D AF [33,34], we expect the spin density in the cloud to decay as a power law $s_{\rm nl}(r) \propto 1/r^\nu$ in the Neel phase. The value of the exponent ν should differ in different spatial domains, provided by two characteristic scales in the problem. The first scale is determined by the impurity spin-flip energy [34], $r_A \sim 1/\lambda|\phi_0| \propto 1/\lambda|\Delta|$, here ϕ_0 is the vacuum expectation value of ϕ field in the Neel phase. The second scale $r_H \sim 1/m_H \sim 1/|\Delta|$ is given by the energy gap of the longitudinal mode. Subscripts A and H stand for Adler and Higgs. For weak coupling, $r_A > r_H$. In the region $r < r_H$, we expect the same exponent for the magnetization decay, $s_{\rm nl}(r) \propto 1/r^3$, as on the disordered side of the QCP. To put it in another way, at small distances $r < r_H$, only magnons with large momenta are relevant, which do not "know" the difference between the spontaneously broken and the paramagnetic phases. On the other hand, at distances $r > r_A$, Adler's theorem for the impurity-magnon vertex is valid and hence the magnetization cloud decays faster than $1/r^3$—we expect that it decays as $1/r^5$. A crossover between the two decay laws is within the range $r_H < r < r_A$. At the QCP, both scales diverge, which means the region with $s_{\rm nl}(r) \propto 1/r^3$ is unlimitedly extending at $|\Delta| \to 0$. This is the same behavior as in the disordered phase.

C. Semiclassical limit: impurity with large spin

From theoretical point of view, it is interesting to consider the semiclassical case of large spin of the impurity. Taking the formal limit $S \to \infty$ in Eqs. (36), (37), and (41), we obtain

$$S_{\rm imp} = S, \quad s_{\rm nl}(r) = 0, \quad \langle\phi(r)\rangle = -\lambda\frac{e^{-\Delta r}}{4\pi r}. \tag{44}$$

We see from Eq. (44), that in the semiclassical limit there is no nonlocal spin density around the impurity and the local spin S is "unscreened" in this case. Therefore there is no spin-charge separation in the semiclassical limit.

Note that the local impurity spin, the nonlocal spin density, and the staggered magnetization in the semiclassical limit are provided just by a tree-level approximation. The reason is that quantum fluctuations of the impurity spin are suppressed at large S. Indeed, let us consider the case of the impurity in the state with the maximal projection of spin on the quantization axis z: $|S, S_z = S\rangle$. The interaction of the impurity with a magnon either leaves projection S_z unchanged or changes it by unity, $\Delta S_z = -1$. The action of operator $\hat{S}_z$ on the state $|S,S\rangle$ provides the eigenvalue S. On the other hand, the matrix element of the lowering operator $\hat{S}_-$ between states $|S,S-1\rangle$ and $|S,S\rangle$ is equal to $\sqrt{2S}$. Therefore processes with a change of the projection of the impurity spin are suppressed in the limit of large S.

In the semiclassical limit, only the z component of the operator of the impurity spin is relevant, as a result the Lagrangian in Eq. (4), corresponding to the interaction of the impurity with magnons, takes the form

$$\mathcal{L}_{\rm int} = -\lambda\psi^\dagger\psi\phi_z. \tag{45}$$

Thus the problem of a classical impurity "dressed" with z-polarized magnons is equivalent to the problem of an impurity interacting with a scalar bosonic field ϕ_z.

The problem of interaction between an impurity and a scalar boson field is known as an independent boson model; this model is exactly solvable [35]. The exact solution agrees with Eq. (44).

The retarded Green's function of the impurity in time representation at $t > 0$ reads [35]

$$G(t) = -i\exp\left[it\epsilon_0 - \lambda^2\sum_{\boldsymbol{q}}\frac{(1-e^{-i\omega_q t})}{2\omega_q^3}\right], \tag{46}$$

where $\epsilon_0 = -\lambda^2\sum_q 1/2\omega_q^2$. Performing a Fourier transformation of the impurity Green's function (46), and calculating the quasiparticle residue at the Green's function pole $\epsilon = \epsilon_0$, we obtain

$$Z = \exp\left(-\lambda^2\sum_q\frac{1}{2\omega_q^3}\right) = \left(\frac{\Delta}{\Lambda}\right)^{\lambda^2/4\pi^2}. \tag{47}$$

In the limit $S \to \infty$, the RG result (34) is consistent with Eq. (47).

V. DISCUSSION OF RESULTS AND CONCLUSION

The present paper has considered a single impurity with spin S embedded into a 3D AF system. The system is close to the O(3) quantum critical point (QCP) separating paramagnetic from the Neel phase. The impurity spin induces the usual magnetization and the staggered magnetization clouds around the position of the impurity. Using the effective Lagrangian method and approaching the QCP from the disordered phase, we have calculated spatial distributions of the spin density $s(r)$ (magnetization) and the staggered magnetization $\langle\phi(r)\rangle$ in the cloud. For the calculations, we use two different

methods, the self-consistent Born approximation (SCBA) and the renormalization group (RG). SCBA is justified by the small parameter $1/N$ where $N = 3$ for the O(3) group, while RG is justified by the small coupling constant. We show that for $S = 1/2$, the results of both methods are consistent within the expected accuracy $1/N$. However, at larger values of the impurity spin, the SCBA method is not valid because the small parameter $1/N$ is compensated by the large spin. Therefore, for $S \geqslant 1$, only the RG results are valid.

The impurity quasiparticle residue vanishes at the QCP, see Eq. (34). This is the first indication that the impurity spin is fully transferred to the magnon cloud. The screening of the impurity spin by spin-one magnetic fluctuations is a Kondo-like effect in a bosonic sector [16]. The spin density has a local component $S_{\rm imp}\delta(\boldsymbol{r})$, which is localized at the site of the impurity, as well as a spatially distributed nonlocal part $s_{\rm nl}(r)$. As a result of the vanishing residue, the impurity's average spin $S_{\rm imp}$ logarithmically vanishes at the QCP, see Eq. (34). Of course, the total spin S is conserved and it is transferred into the nonlocal spin cloud. The nonlocal spin density at $r < 1/\Delta$, where Δ is the magnon gap, decays as $s_{\rm nl}(r) \propto 1/r^3$ with proper logarithmic corrections, see Eq. (41). Obviously, at $r > 1/\Delta$, the spin density decays exponentially.

Spin in the nonlocal cloud is mainly accumulated at large distances $r \simeq 1/\Delta$, see Eq. (42). Therefore the spin is spatially separated from the impurity and at $\Delta \to 0$ the separation scale becomes infinite. In this sense, our results demonstrate the spin-charge separation in 3D magnetic systems at the QCP.

Interestingly, the cloud of the staggered magnetization at $r < 1/\Delta$ decays only as the first power of distance, see Eq. (37). This is why a tiny concentration of impurities can significantly influence the critical behavior of the system.

Finally, we have analyzed the semiclassical limit of a very large impurity spin, $S \gg 1$. In this limit, the quantum spin-flip transitions become negligible and the spin impurity problem is reduced to an exactly solvable textbook example [35].

ACKNOWLEDGMENTS

We gratefully acknowledge A. Milstein and H. Scammell for useful discussions. This research was supported by Australian Research Council (Grant No. DP110102123).

[1] S. Sachdev and B. Keimer, Phys. Today **64**, 29 (2011).
[2] H. Tanaka, K. Goto, M. Fujisawa, T. Ono, and Y. Uwatoko, Physica (Amsterdam) **329-333B**, 697 (2003).
[3] A. Oosawa, M. Fujisawa, K. Kakurai, and H. Tanaka, Phys. Rev. B **67**, 184424 (2003).
[4] H. Imamura, T. Ono, K. Goto, and H. Tanaka, Phys. Rev. B **74**, 064423 (2006).
[5] T. Suzuki, I. Watanabe, F. Yamada, Y. Ishii, K. Ohishi, Risdiana, T. Goto, and H. Tanaka, Phys. Rev. B **80**, 064407 (2009).
[6] T. Suzuki, M. Yamada, Y. Ishii, I. Watanabe, T. Goto, H. Tanaka, and K. Kubo, Phys. Rev. B **83**, 174436 (2011).
[7] A. W. Sandvik, E. Dagotto, and D. J. Scalapino, Phys. Rev. B **56**, 11701 (1997).
[8] M. Hase, I. Terasaki, Y. Sasago, K. Uchinokura, and H. Obara, Phys. Rev. Lett. **71**, 4059 (1993).
[9] J. Bobroff, N. Laflorencie, L. K. Alexander, A. V. Mahajan, B. Koteswararao, and P. Mendels, Phys. Rev. Lett. **103**, 047201 (2009).
[10] M. Vojta, C. Buragohain, and S. Sachdev, Phys. Rev. B **61**, 15152 (2000).
[11] K. H. Höglund, A. W. Sandvik, and S. Sachdev, Phys. Rev. Lett. **98**, 087203 (2007).
[12] Rong Yu, Omid Nohadani, Stephan Haas, and Tommaso Roscilde, Phys. Rev. B **82**, 134437 (2010).
[13] Y. Saito, A. Koga, and N. Kawakami, J. Phys. Soc. Jpn. **72**, 1208 (2003).
[14] V. Barzykin and I. Affleck, Phys. Rev. B **57**, 432 (1998).
[15] K. Ingersent and Q. Si, Phys. Rev. Lett. **89**, 076403 (2002).
[16] S. Florens, L. Fritz, and M. Vojta, Phys. Rev. Lett. **96**, 036601 (2006).
[17] S. I. Tomonaga, Prog. Theor. Phys. **5**, 544 (1950).
[18] J. M. Luttinger, J. Math. Phys. **4**, 1154 (1963).
[19] W. O. Putikka, R. L. Glenister, R. R. P. Singh, and H. Tsunetsugu, Phys. Rev. Lett. **73**, 170 (1994).
[20] Y. C. Chen, A. Moreo, F. Ortolani, E. Dagotto, and T. K. Lee, Phys. Rev. B **50**, 655 (1994).
[21] T. Tohyama and S. Maekawa, J. Phys. Soc. Jpn. **65**, 1902 (1996).
[22] G. B. Martins, R. Eder, and E. Dagotto, Phys. Rev. B **60**, R3716 (1999).
[23] M. Holt, J. Oitmaa, W. Chen, and O. P. Sushkov, Phys. Rev. B **87**, 075109 (2013).
[24] O. Nohadani, S. Wessel, and S. Haas, Phys. Rev. B **72**, 024440 (2005).
[25] S. Jin and A. W. Sandvik, Phys. Rev. B **85**, 020409(R) (2012).
[26] J. Zinn-Justin, *Quantum Field Theory and Critical Phenomena*, 3rd ed. (Oxford University Press, Oxford, 1996).
[27] A. I. Milstein and O. P. Sushkov, Phys. Rev. B **84**, 195138 (2011).
[28] Y. A. Kharkov, O. P. Sushkov (unpublished).
[29] O. P. Sushkov, Phys. Rev. B **62**, 12135 (2000).
[30] S. A. Brazovskii and I. A. Lukyanchuk, Zh. Eksp. Teor. Fiz. **96**, 2088 (1989) [Sov. Phys. JETP **69**, 1180 (1989)].
[31] R. R. Ramazashvili, Phys. Rev. Lett. **101**, 137202 (2008); Phys. Rev. B **79**, 184432 (2009).
[32] A. I. Milstein and O. P. Sushkov, Phys. Rev. B **78**, 014501 (2008).
[33] V. Yu. Irkhin, A. A. Katanin, and M. I. Katsnelson, Phys. Rev. B **60**, 14779 (1999).
[34] A. Lüscher and O. P. Sushkov, Phys. Rev. B **71**, 064414 (2005).
[35] G. D. Mahan, *Many-Particle Physics* (Kluwer Academic/Plenum Publishers, New York, 2000), pp. 218–247.